Supporting Information

Cellulose Hierarchical Sponge-Aerogel Fibers via Ionic Liquid-Assisted Coaxial Wet Spinning: Lightweight Architectures for Gas Detection and Adaptive Thermal Management

Jinzhu Huang [a], Hanguang Wu [b], Zhiqiang Su [a]**

[a] State Key Laboratory of Chemical Resource Engineering, Beijing Key Laboratory of Advanced Functional Polymer Composites, Beijing University of Chemical Technology, Beijing 100029, China.

[b] Beijing Key Laboratory of Clothing Materials R & D and Assessment, Beijing Institute of Fashion Technology, Beijing 100029, China.

*Corresponding authors.

E-mail: hanguangwu&bift.edu.cn (H. Wu), suzq&mail.buct.edu.cn (Z. Su)

Table of contents

1. Supplementary Figures

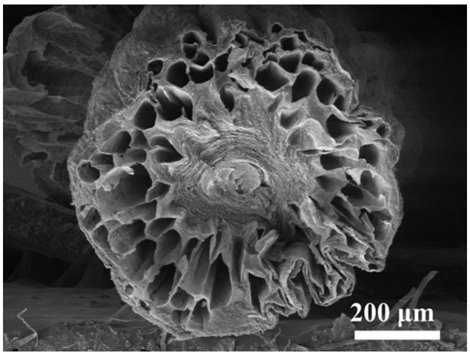

Fig. S1 Cross-sectional SEM image of MPC aerogel fiber.

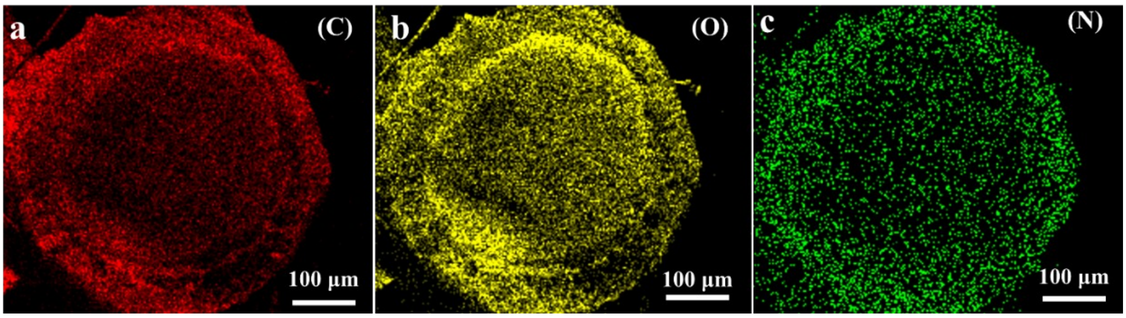

Fig. S2 EDS elemental dispersion diagrams of MPC&C sponge-aerogel microfiber (a) C, (b) O, (c) N.

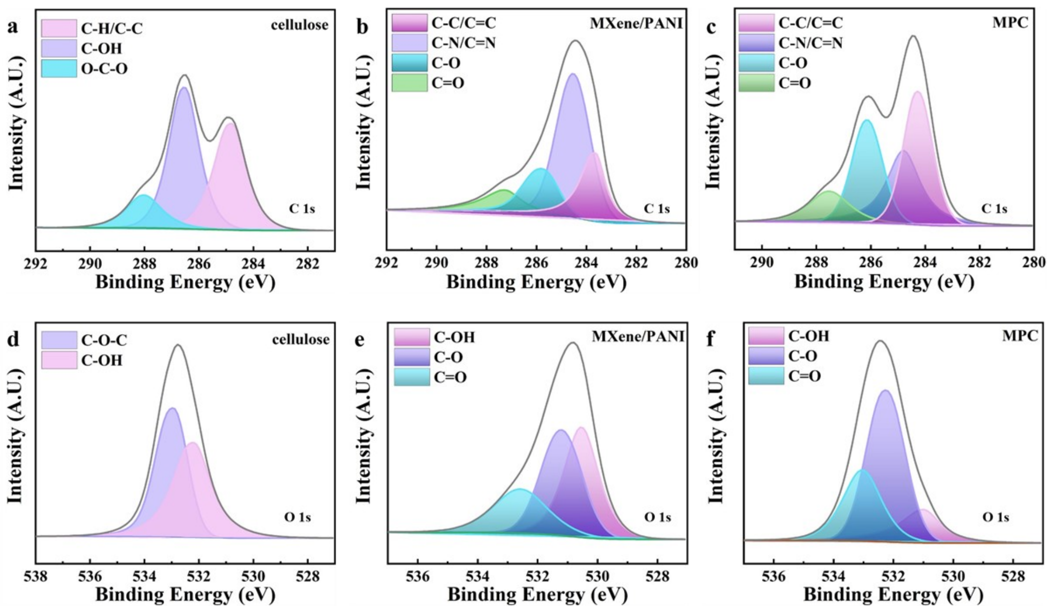

Fig. S3 (a-c) The C 1s XPS spectra of the cellulose, the MXene/PANI, and the MPC. (d-f) The O 1s XPS spectra of the cellulose, the MXene/PANI, and the MPC.

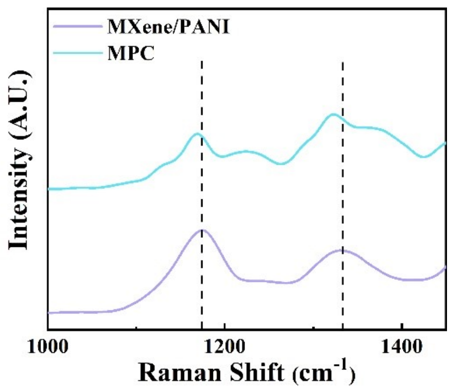

Fig. S4 The Raman spectra of the MXene/PANI and the MPC.

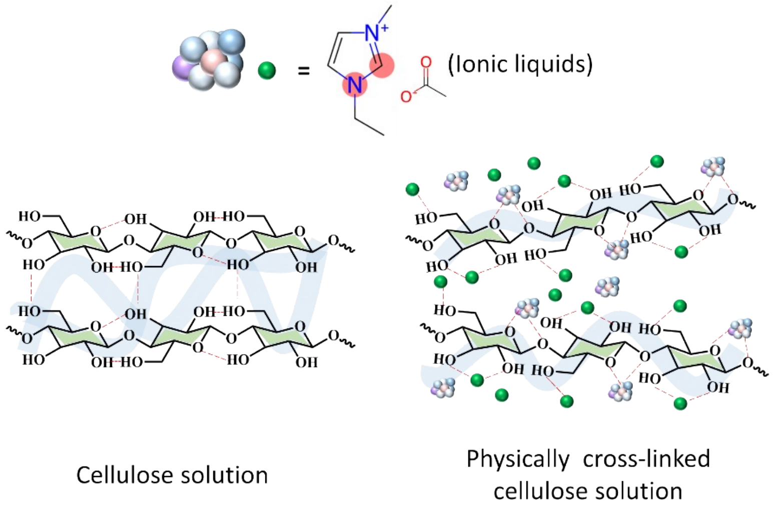

Fig. S5 Schematic diagram of the dissolution mechanism of cellulose in ionic liquids.

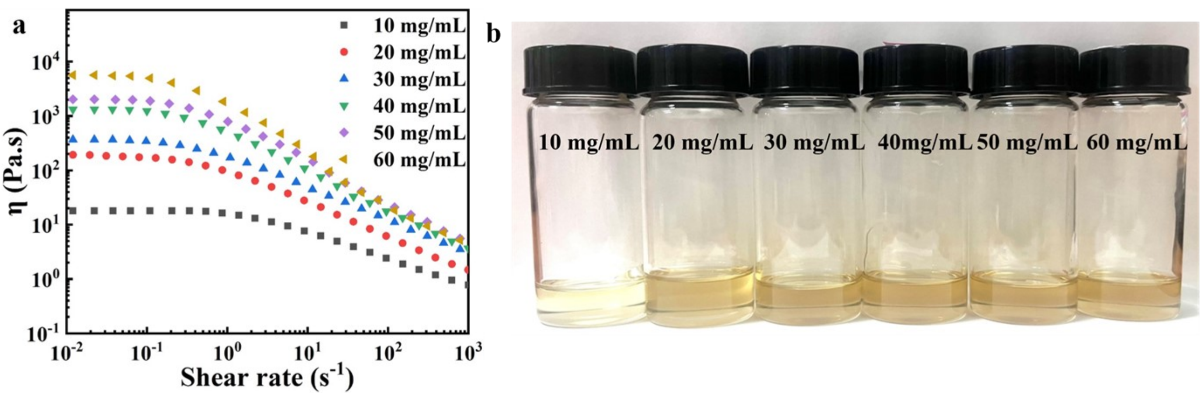

Fig. S6 (a) Log−log plots of the apparent viscosity of spinning solutions as a function of shear rate for different cellulose contents. (b) Optical images of spinning solutions with different cellulose contents.

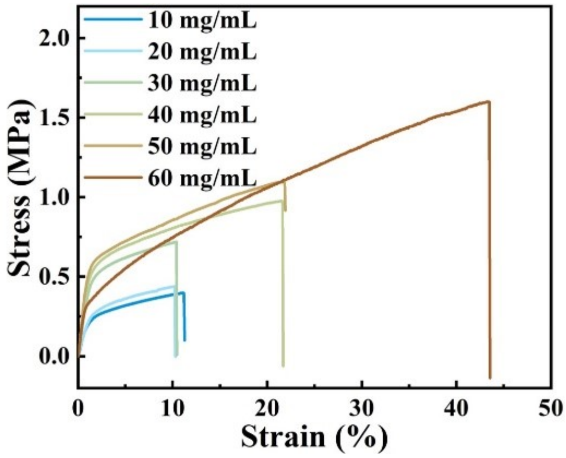

Fig. S7 Stress-strain curves of cellulose aerogel fibers prepared by using the solution with different cellulose contents (10-60 mg/mL).

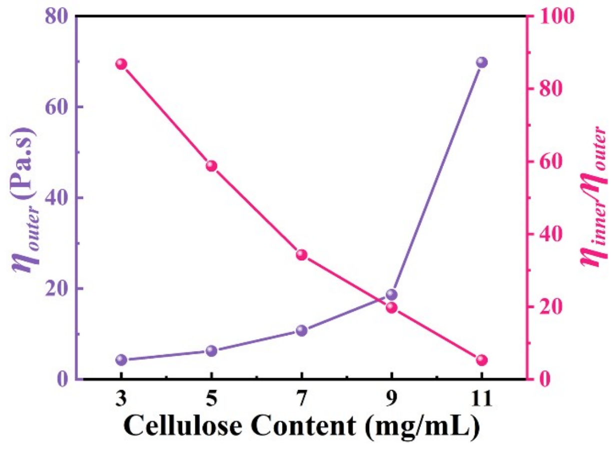

Fig. S8 Outer fluid viscosity and the viscosity ratio of inner and outer fluids with different cellulose contents in the outer layer (at the shear rate of 0.01 s^{-1}).

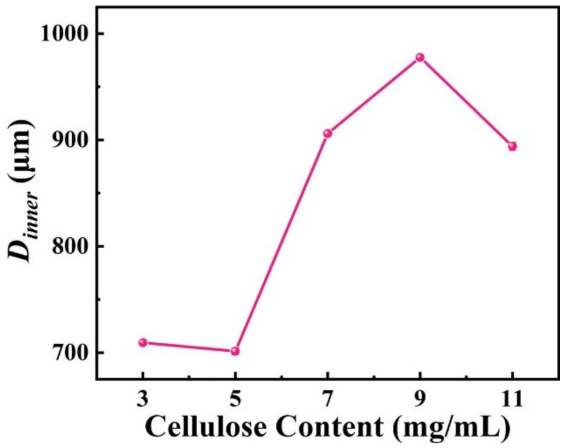

Fig. S9 Effect of different cellulose contents in the outer fluid on the inner diameter of MPC&C sponge-aerogel microfibers.

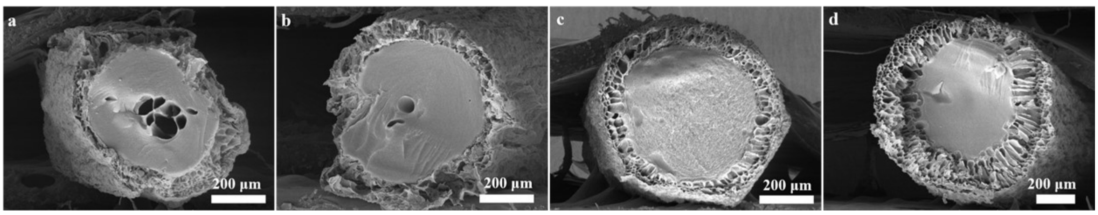

Fig. S10 SEM images of MPC&C sponge-aerogel microfiber cross sections in the outer fluid with different cellulose contents: (a) 5 mg/mL; (b) 7 mg/mL; (c) 9 mg/mL; (d) 11 mg/mL.

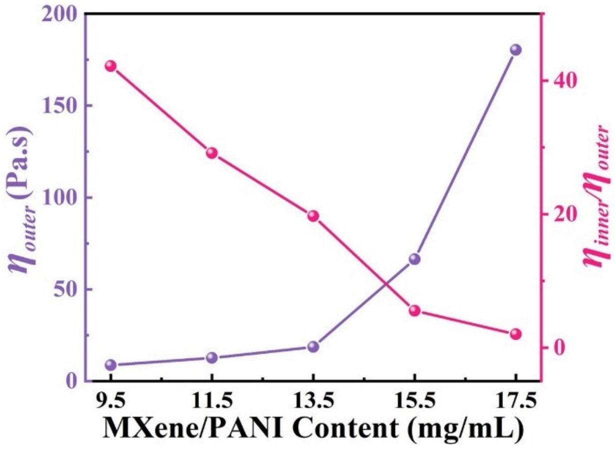

Fig. S11 Outer fluid viscosity and the viscosity ratio of inner and outer fluids with different MXene/PANI contents in the outer layer (at the shear rate of 0.01 s^{-1}).

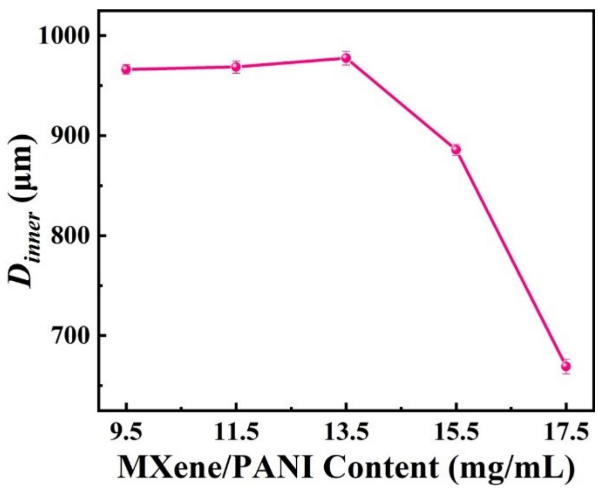

Fig. S12 Effect of different MXene/PANI contents in the outer fluid on the inner diameter of MPC&C sponge-aerogel microfibers.

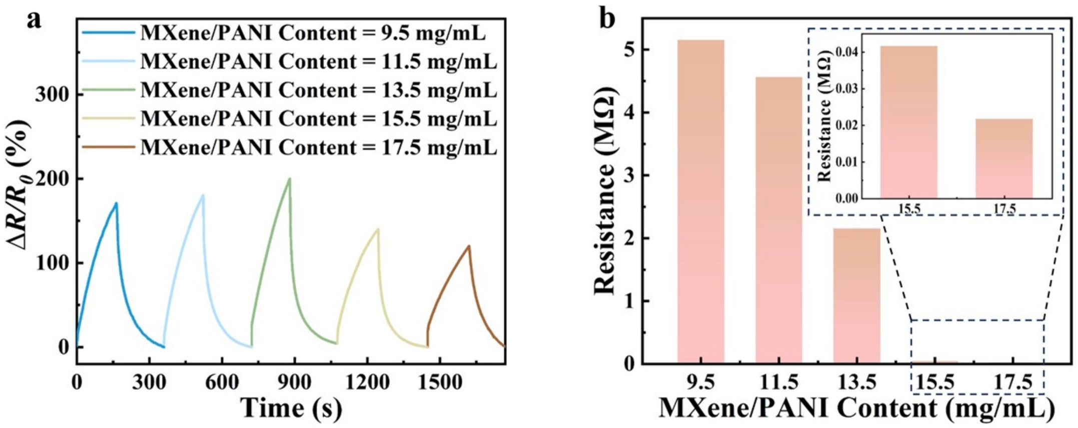

Fig. S13 (a) Sensing response of MPC&C sponge-aerogel microfibers with different MXene/PANI contents (9.5, 11.5, 13.5, 15.5, 17.5 mg/mL) at 100 ppm NH_3 (at 20℃ and 45% RH). (b) The resistance of MPC&C sponge-aerogel microfibers with different MXene/PANI contents in the outer layer.

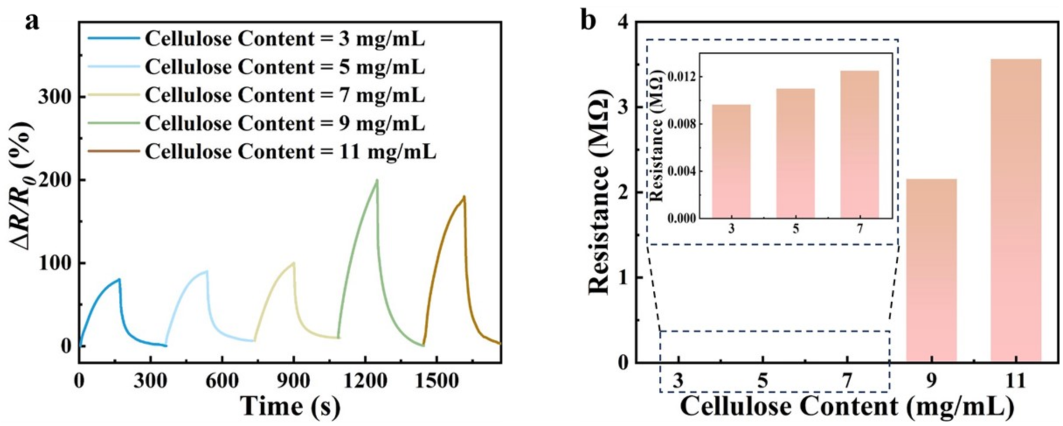

Fig. S14 (a) Sensing response of MPC&C sponge-aerogel microfibers with different cellulose contents (3, 5, 7, 9, 11 mg/mL) at 100 ppm NH_3 (at 20℃ and 45% RH). (b) The resistance of MPC&C sponge-aerogel microfibers with different cellulose contents in the outer layer.

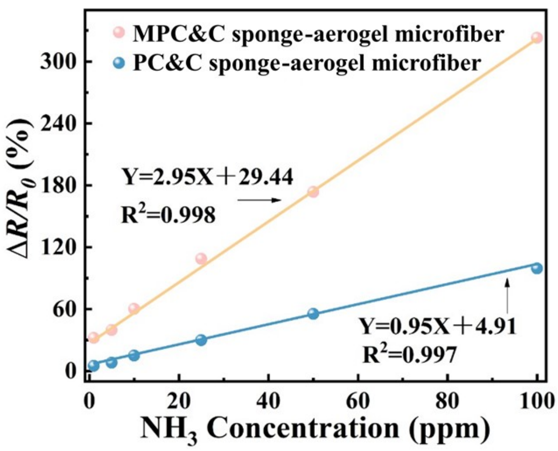

Fig. S15 The linear fitting curves for the response of MPC&C sponge-aerogel microfiber and PC&C sponge-aerogel microfiber at exposure to 1-100 ppm NH_3.

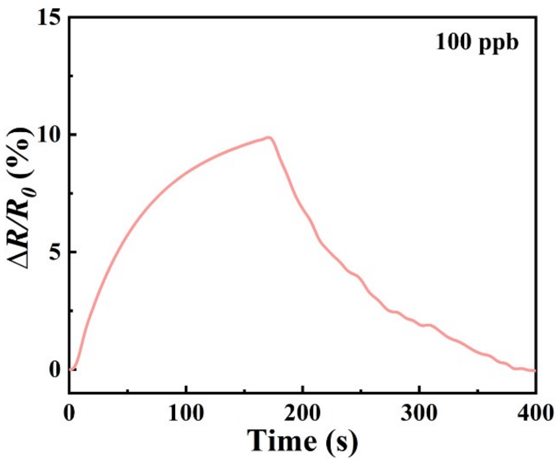

Fig. S16 Sensing response of MPC&C sponge-aerogel microfiber at 100 ppb NH_3 concentration.

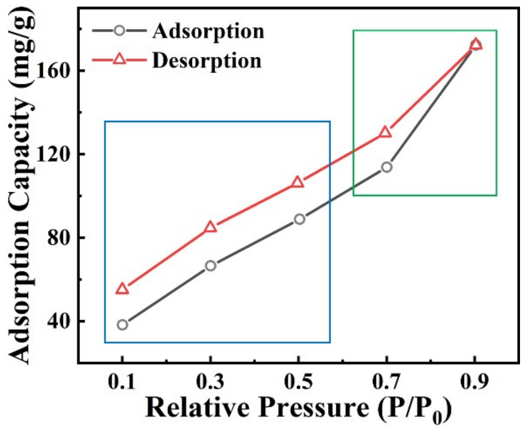

Fig. S17 Absorption-desorption isotherm of the MPC&C sponge-aerogel microfiber with in situ humidity-controlled (10% RH, 30% RH, 50% RH, 70% RH, 90% RH).

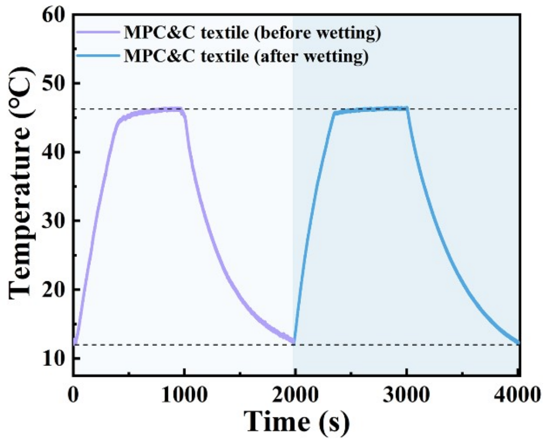

Fig. S18 Comparison of the thermal insulation property of the MPC&C textile before and after wetting.

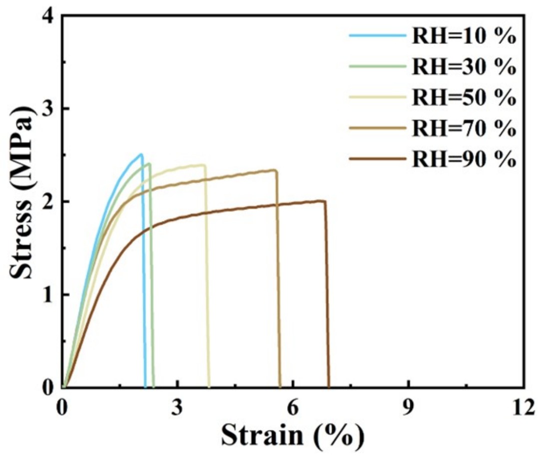

Fig. S19 Stress-strain curves of MPC&C sponge-aerogel microfiber at 10% RH, 30% RH, 50% RH, 70% RH, and 90% RH.

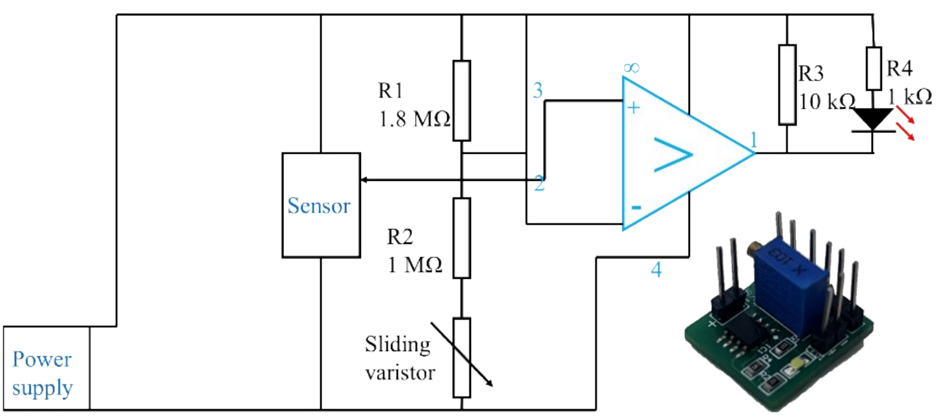

Fig. S20 Circuit design of light-emitting diode (LED) for NH_3 alarm.

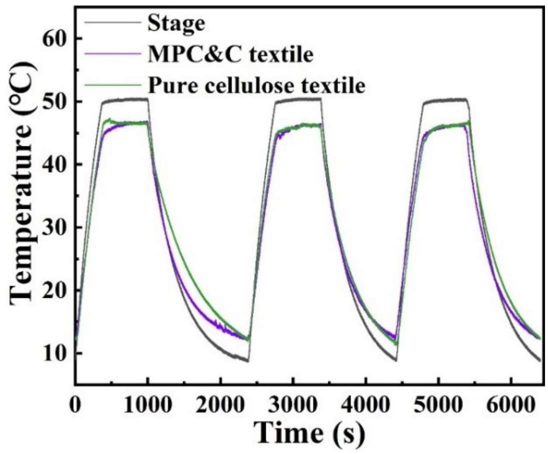

Fig. S21 Comparison of the thermal insulation property between the MPC&C textile and the textile woven by the pure cellulose aerogel fibers.

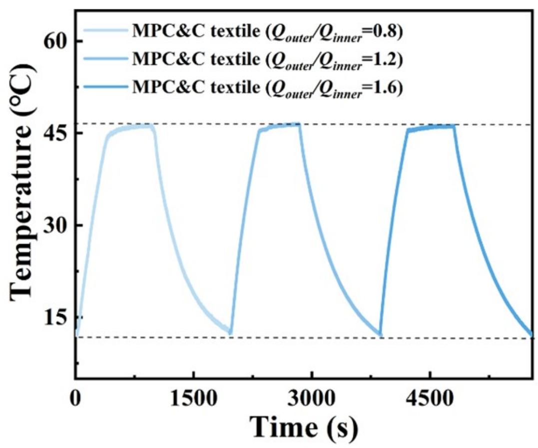

Fig. S22 Comparison of the thermal insulation property between the MPC&C textile prepared by different flow rate ratios.

2. Supplementary Tables

Table S1 Performances comparison of MPC&C sponge-aerogel microfiber with other cellulose-based NH_3 sensors.

	Sensing Response (%)	Limit of Detection (ppb)	Response Time (s)	Morphology	Ref.
BC/MXene Bioaerogel NH_3 Sensor	70% at 20 ppm	20000	34 s at 20 ppm	Block Aerogel	S1
MXene/PANI/BC Aerogel NH_3 Sensor	27.6% at 2.5 ppm	2500	270 s at 2.5 ppm	Block Aerogel	S2
P/AC/P NH_3 Sensor	20.2% at 1 ppm	30	4.8 s at 1 ppm	Membrane	S3
LCNF/RGO/PANI NH_3 Sensor	11% at 1 ppm	1000	1500 s at 1 ppm	Membrane	S4
PANI/Cellulose NH_3 Sensor	2.49% at 1 ppm	600	10 s at 1 ppm	Fiber	S5
MPC&C Sponge-Aerogel Microfiber NH_3 Sensor	32% at 1 ppm	100	112 s at 1 ppm	Aerogel Fiber	**This work**

Table S2 Comparison of MPC&C sponge-aerogel microfibers with other cellulose-based aerogel fibers.

Sample	Functionality	Fabrication Technique	Specific Strength (N·m/kg)	Thermal Conductivity (W m^{-1} K^{-1})	Ref.
CAF/BKTMS Aerogel Fiber	Thermochromic	Wet Spinning & Hydrophobic Coating	0.0114	0.074	S6
BC/HCNT Aerogel Fiber	Photothermal Conversion	Wet Spinning & Silane Gelation	0.0112	-	S7
HCCAF Aerogel Fiber	Motion Sensing	Wet-spinning Process	0.0132	0.048	S8
CAF Aerogel Fiber	Flame Retardant	Wet Spinning & Chemical Crosslinking	0.0069	0.073	S9
PAN@CNF/MWCNT Aerogel Fiber	Phase Change Energy Storage	Coxial Wet Spinning Process	0.0171	0.049	S10
MPC&C Sponge-Aerogel Microfiber	NH_3 Sensing	Coaxial Wet Spinning Process	0.0072	0.064	**This Work**

References:

S1 X. Jin, L. Li, S. Zhao, X. Li, K. Jiang, L. Wang and G. Shen, *ACS Nano*, 2021, **15**, 18385-18393.

S2 H. Zhi, X. Zhang, F. Wang, P. Wan and L. Feng, *ACS Appl. Mater. Interfaces.*, 2021, **13**, 45987-45994.

S3 Y. Zhou, R. Zhang, X. She, J. Li, H. Zhao, Y. Wang, Y. Chen, L. Xie, C. Zou and X. Li, *ACS Appl. Mater. Interfaces.*, 2023, **15**, 53802-53814.

S4 N. R. Tanguy, K. Khorsand Kazemi, J. Hong, K. C. Cheung, S. Mohammadi, P. Gnanasekar, S. S. Nair, M. H. Zarifi and N. Yan, *Carbohydr. Polym.*, 2022, **278**, 118920.

S5 C. Wang, Y. Liao, H.-Y. Yu, Y. Dong and J. Yao, *Carbohydr. Polym.*, 2023, **319**, 121175**.**

S6 S. Jiang, W. Yan, C. Cui, W. Wang, J. Yan, H. Tang and R. Guo, *ACS Appl. Mater. Interfaces.*, 2023, **15**, 47577-47590.

S7 D. Zhang, Q. Liang, T. Zhang, M. Guan, H. Wang and S. Chen, *Adv. Funct. Mater.*, 2024, **35**, 2413361.

S8 Y. Chen, C. Zhang, S. Tao, H. Chai, D. Xu, X. Li and H. Qi, *Chem. Eng. J.*, 2023, **466**, 143453.

S9 S. Jiang, S. Jiang, J. Yan, C. Lin, W. Wang, S. Jiang, L. Cao and R. *Guo, Ind. Eng. Chem. Res.*, 2024, **63**, 15301-15313.

S10 W. Mu, H. Cao, X. Cui, Z. Xu, T. Zhang and Y. Zhao, *ACS Appl. Polym. Mater.*, 2024, **6**, 15162-15171.